

# Direct time-domain observation of transition from strong to weak coupling in a semiconductor microcavity

Shudong Jiang,<sup>a)</sup> Susumu Machida, Yoshihiro Takiguchi, and Yoshihisa Yamamoto<sup>b)</sup>  
*ERATO Quantum Fluctuation Project, NTT Musashino R&D Center, 3-9-11 Midori-cho, Musashino-shi,  
 Tokyo 180, Japan*

Hui Cao

*Department of Physics and Astronomy, Northwestern University, Evanston, Illinois 60208-3112*

(Received 6 July 1998; accepted for publication 20 September 1998)

We measured temporal evolution of the coherent emission from a semiconductor microcavity by a very sensitive ac balanced homodyne detection system. The experimental results can be well explained by the coupled exciton-photon model with varying exciton linewidth. © 1998 American Institute of Physics. [S0003-6951(98)00347-7]

In the past few years there has been much interest and study of the coupled exciton-photon system in a quantum well (QW) embedded semiconductor microcavity.<sup>1-4</sup> In the weak coupling regime, the radiation pattern and the decay rate of excitonic spontaneous emission can be drastically modified by a resonant microcavity.<sup>5</sup> In the strong coupling regime, new eigenstates of the system, i.e., the exciton-polariton states are formed.<sup>6</sup> The normal mode splitting and corresponding temporal oscillation of the emission have been observed in the absorption/emission spectra<sup>7-9</sup> and in the temporal measurement<sup>10-13</sup> at low excitation intensity. At high pump power, the rapid dephasing of excitons and bleaching of excitonic oscillator strength induce a transition from strong coupling to weak coupling.<sup>14-17</sup> In this letter, we report direct observation of such transition in the time domain.

In our microcavity sample grown by molecular beam epitaxy, a 20 nm GaAs QW is located in the middle of a half-wavelength distributed Bragg reflector (DBR) cavity. The top (bottom) mirror consists of 15.5 (30) pairs of Al<sub>0.15</sub>Ga<sub>0.85</sub>As and AlAs layers. The Al<sub>0.3</sub>Ga<sub>0.7</sub>As buffer layer is tapered along one direction of the sample so that the cavity resonant photon frequency varies with sample position. The sample was cooled down to 4.2 K in a liquid helium cryostat during the optical measurement.

The temporal evolution of the microcavity emission was measured by an ac balanced homodyne detection system.<sup>18</sup> 150 fs pulses from a mode-locked Ti:sapphire laser were split by a beam splitter into two arms of a modified Mach-Zehnder interferometer. One beam was used as the local oscillator wave, the other was used to resonantly excite the microcavity sample at an incident angle of 2.5°. The reflected pulses and the microcavity emission into the reflection direction were combined with the local oscillator pulses at a second beam splitter. The two outputs from the second beam splitter were detected by two identical photodetectors, whose photocurrents were fed into a differential amplifier.

The intensity noise of the local oscillator was reduced by 35 dB due to the common mode rejection of the balanced homodyne detector. To eliminate the instability of the interferometer, the optical path of the signal arm was modulated with  $\Delta l$  at a frequency  $\nu_l$  by a mirror mounted on a piezoelectric transducer (PZT) scanner. This optical path length modulation generates a sinusoidal signal in the differential amplifier output at a frequency  $\nu_m = \nu_l \times \Delta l / \lambda$ , where  $\lambda$  is the center wavelength of the optical pulses. Since this ac balanced homodyne detection scheme is insensitive to the long-term drift and short-term instability of the Mach-Zehnder interferometer, it gives ultrahigh sensitivity. The time delay  $\tau$  of the local oscillator pulses can be varied by moving a corner mirror placed on a translational stage. The time evolution of the amplitude of the coherent emission from the microcavity was detected by measuring the sinusoidal output signal at frequency  $\nu_m$  at different time delay  $\tau$  by a narrow bandpass filter and an ac voltage meter.

Figure 1(a) shows the temporal evolution of the micro-

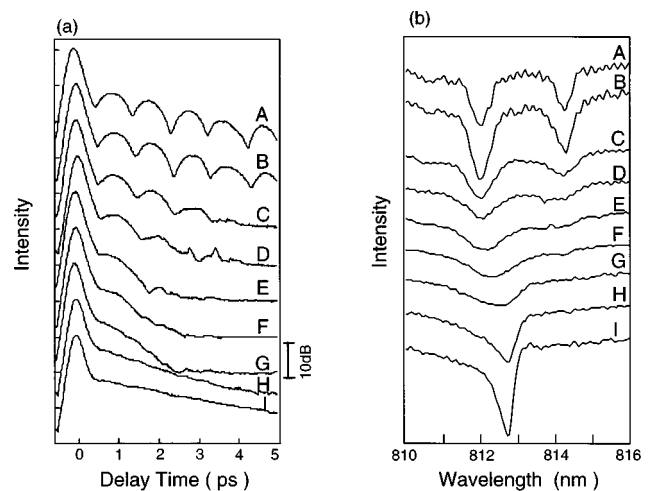


FIG. 1. (a) Measured temporal evolution of the microcavity emission at different pump power. (b) Simultaneous measurement of the reflection spectra from the microcavity at different pump power. The estimated exciton densities in the microcavity are (A)  $1.1 \times 10^8 \text{ cm}^{-2}$ ; (B)  $1.1 \times 10^9 \text{ cm}^{-2}$ ; (C)  $5.5 \times 10^9 \text{ cm}^{-2}$ ; (D)  $1.1 \times 10^{10} \text{ cm}^{-2}$ ; (E)  $2.0 \times 10^{10} \text{ cm}^{-2}$ ; (F)  $2.7 \times 10^{10} \text{ cm}^{-2}$ ; (G)  $4.4 \times 10^{10} \text{ cm}^{-2}$ ; (H)  $6.6 \times 10^{10} \text{ cm}^{-2}$ ; (I)  $1.1 \times 10^{11} \text{ cm}^{-2}$ , respectively.

<sup>a)</sup>Electronic mail: sjiang@yqfp.jst.go.jp

<sup>b)</sup>Also with NTT Basic Research Laboratory, 3-1 Wakamiya, Atsugi, Kanagawa, 243, Japan and E. L. Ginzton Laboratory, Stanford University, Stanford, CA 94305.

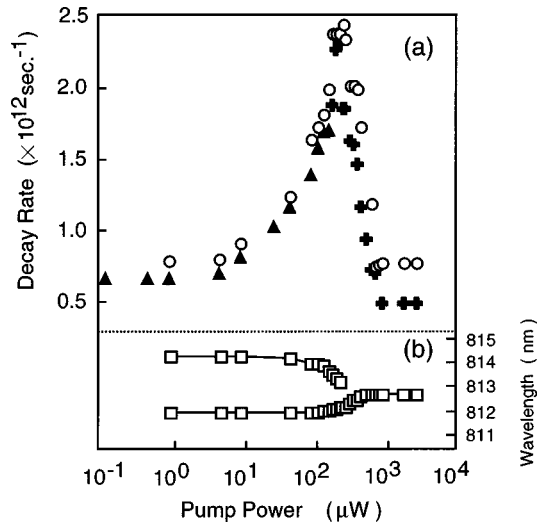


FIG. 2. Measured decay rate and peak wavelength in the reflection spectra of the microcavity emission as a function of the pump power. (a) Measured decay rate. (b) Measured peak wavelength in the reflection spectra.

cavity emission at different pump power. The peak at  $\tau=0$  corresponds to the direct reflection of the pump pulses from the sample surface, while the subsequent peaks correspond to the exciton–polariton oscillation. In the following analysis, we used the first peaks as the zero time markers and exclude it from evaluating the decay rates of the microcavity emission. The spot size of the pump beam on the sample was about  $25 \mu\text{m}$  in diameter. The spectra of the pump pulses were centered at 814 nm (1526.26 meV) with a full width at half maximum of 9 nm (17 meV). The cavity photon frequency was tuned close to the QW heavy-hole (HH) exciton emission frequency. The exciton densities are (A)  $1.1 \times 10^8 \text{cm}^{-2}$ ; (B)  $1.1 \times 10^9 \text{cm}^{-2}$ ; (C)  $5.5 \times 10^9 \text{cm}^{-2}$ ; (D)  $1.1 \times 10^{10} \text{cm}^{-2}$ ; (E)  $2.0 \times 10^{10} \text{cm}^{-2}$ ; (F)  $2.7 \times 10^{10} \text{cm}^{-2}$ ; (G)  $4.4 \times 10^{10} \text{cm}^{-2}$ ; (H)  $6.6 \times 10^{10} \text{cm}^{-2}$ ; and (I)  $1.1 \times 10^{11} \text{cm}^{-2}$ . Figure 1(b) shows the simultaneous measurement of the reflection spectra of a probe beam. At low pump power, the strong coupling of the QW HH exciton with the cavity photon results in two HH exciton–polariton peaks in the reflection spectrum. The beating between these two exciton–polariton states leads to a temporal oscillation of microcavity emission. The oscillation period is about 1.2 ps, which is in good agreement with the spectral splitting of about 2.1 nm (4.1 meV) between the two HH exciton–polariton states. As we increase the excitation intensity, in the frequency domain, the exciton–polariton peaks are broadened, and their mode splitting is slightly reduced. In the time domain, the microcavity emission peak intensity decays faster, but the exciton–polariton oscillation becomes slower. Eventually, the two exciton–polariton peaks in the reflection spectra are replaced by a single cavity photon peak, indicating the transition from strong exciton–photon coupling to weak coupling. The single cavity photon resonance narrows as the pump power increases. Meanwhile, the temporal oscillation of the microcavity emission is replaced by an exponential decay. The decay rate decreases as the pump power increases.

Figure 2 shows the measured decay rate and peak wavelength in the reflection spectra of the microcavity emission as a function of the pump power. Since the pump pulse's dura-

tion is much shorter than the decay time of the microcavity emission, in the strong coupling regime, we extracted the exciton–polariton decay rate from the slope of the oscillation peaks in Fig. 1(a), i.e., fitting the height of the oscillation peaks by an exponential function. In the weak coupling regime, we obtained the emission decay rate by fitting the intensity with an exponential function.

In Fig. 2(a), triangles represent the decay rates in the strong coupling regime at low pump power, while crosses are the decay rates in a weak coupling regime at high pump power. The circles represent the decay rates  $\gamma_T$  evaluated from the spectral linewidth  $\Delta\omega$  of the reflection spectrum by using the relation  $\gamma_T = \Delta\omega/2$ . It is clear that the decay rates evaluated from the temporal evolution are in close agreement with those from the corresponding spectral linewidth. As the pump power increases, the decay rate of the exciton–polariton oscillation increases. At the transition point from strong coupling to weak coupling, the decay rate is maximum. After passing the transition point, as the pump power increases further, the exponential decay rate of the microcavity emission starts decreasing. Figure 2(b) shows the peak wavelength in the reflection spectra as a function of the pump power.

To understand our experimental results, we have set up a simple model based on the Hamiltonian:

$$H = \hbar\omega_c(a^\dagger a + \frac{1}{2}) + \hbar\omega_h(b^\dagger b + \frac{1}{2}) + \hbar g(a^\dagger b + ab^\dagger) + \sum_k \hbar g_k(a^\dagger c_k + ac_k^\dagger) + \sum_l \hbar g_l(b^\dagger d_l + bd_l^\dagger), \quad (1)$$

where  $a$ , and  $b$  ( $\hbar\omega_c$ , and  $\hbar\omega_h$ ) are the operators (energies) of the cavity photon, and QW HH–exciton, respectively.  $g$  is the coupling constant between the HH–exciton and cavity photon. The fourth and fifth terms in Eq. (1) represent the reservoir coupling of the cavity photon and HH exciton, respectively. We consider the resonant case  $\omega_c = \omega_h$ . Hence, the light-hole (LH) exciton can be neglected since its emission frequency is far from the cavity photon frequency. Heisenberg equations of motion for  $a$  and  $b$  are derived after eliminating the photon and exciton reservoir coordinates and introducing the damping terms  $\Gamma_c$  and  $\Gamma_h$  for the cavity photon and HH exciton, respectively. When  $g < \Gamma_c/2$  or  $\Gamma_h/2$ , the system is in the weak coupling regime, and thus, the exciton–photon coupling can be treated as a perturbation to the uncoupled exciton–photon system. On the other hand, when  $g > \Gamma_c/2$  and  $\Gamma_h/2$ , the system is in the strong coupling regime where new eigenstates of the system, i.e., exciton–polariton states, are formed. At low excitation intensity where the exciton density is much lower than the Mott density, exciton–exciton interaction can be neglected since the average distance between excitons is much larger than the exciton Bohr radius. However, as the exciton density increases, excitons scatter among each other and also with free carriers. The corresponding dephasing leads to an increase of  $\Gamma_h$ . Eventually, when  $\Gamma_h/2$  exceeds  $g$ , the system makes a transition from strong coupling to weak coupling. As the excitation density increases further, phase space filling and screening lead to a reduction of the excitonic oscillator strength, and thus, a decrease of exciton–photon coupling

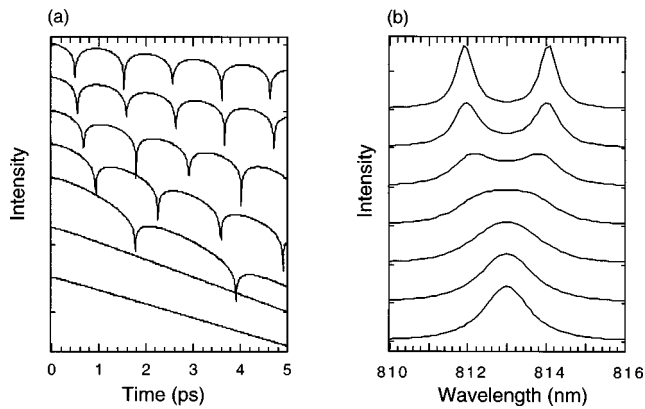


FIG. 3. (a) Calculated temporal evolution of the microcavity emission at different  $\Gamma_h$ . (b) Calculated absorption spectra at different  $\Gamma_h$ . For the curves from the top to the bottom,  $\Gamma_h$  are 1, 2, 4, 6, 8, 10, and 12 meV, respectively.

constant  $g$ . In our simulation, we consider the excitation intensity regime where the reduction of  $g$  is negligible.

Figure 3(b) shows the calculated absorption spectra as a function of  $\Gamma_h$ .<sup>19</sup> We set  $g = 4.1$  meV,  $\Gamma_c = 1$  meV, based on the experimental parameters of our samples. As  $\Gamma_h$  increases, the exciton-polariton peaks are broadened, because the linewidth of exciton-polariton peaks is proportional to the sum of QW exciton linewidth ( $\Gamma_h$ ) and cavity photon linewidth, i.e.,  $(\Gamma_c + \Gamma_h)/2$ . The splitting  $\Omega$  also decreases due to the increase of  $\Gamma_h$  according to

$$\Omega = \sqrt{4g^2 - (\Gamma_h - \Gamma_c)^2}. \quad (2)$$

When  $\Gamma_h/2$  approaches  $g$ , the two exciton-polariton peaks merge into a single broad peak, indicating the transition from strong coupling to weak coupling. As  $\Gamma_h$  increases further, the linewidth of this single peak decreases, eventually approaching the bare photon resonance linewidth  $\Gamma_c$ . This is because in the weak coupling regime, when  $\Gamma_h \gg \Gamma_c$ , the linewidth of the absorption peak is determined mostly by  $\Gamma_c$ . Therefore, our simulation results are consistent with our experimental data.

The time evolution of the microcavity emission was calculated by solving the Heisenberg equation of motion for the cavity field amplitude  $a(t)$ , assuming the initial state is the bare photon state. As shown in Fig. 3(a), when  $\Gamma_h/2$  is smaller than  $g$ , the microcavity emission shows a temporal oscillation. This indicates that the microcavity system oscillates back and forth between QW exciton state and cavity photon state. As  $\Gamma_h$  increases, the oscillation decays faster, because the decay rate of exciton-polariton emission is proportional to  $\Gamma_h + \Gamma_c$ . The oscillation period, which is in-

versely proportional to the exciton-polariton mode splitting  $\Omega$ , slightly increases due to the slight decrease in  $\Omega$  at larger  $\Gamma_h$ . When  $\Gamma_h/2$  approaches  $g$ , the temporal oscillation is replaced by an exponential decay. This change in the time domain is accompanied with the merge of the two exciton-polariton peaks into a single peak in the frequency domain. As  $\Gamma_h$  increases further, the decay rate of the microcavity emission starts decreasing, and eventually it approaches  $\Gamma_c$  in the weak coupling limit. The calculation results agree well with the experimental data.

In conclusion, we observed, in both time and frequency domains, the transition from strong exciton-photon coupling to weak coupling in a semiconductor microcavity. The experimental observation can be well explained by our theoretical model.

<sup>1</sup>Y. Yamamoto and R. E. Slusher, *Phys. Today* **46**, 66 (June 1993).

<sup>2</sup>R. E. Slusher and C. Weisbuch, *Solid State Commun.* **92**, 149 (1994).

<sup>3</sup>*Confined Electrons and Photons*, edited by E. Burstein and C. Weisbuch (Plenum, New York, 1995).

<sup>4</sup>*Spontaneous Emission and Laser Oscillation in Microcavities*, edited by H. Yokoyama and K. Ujihara (CRC, Boca Raton, FL, 1995).

<sup>5</sup>Y. Yamamoto, G. Björk, K. Igeta, and Y. Horikoshi, in *Quantum Optics and Coherence V*, edited by H. H. Eberly, L. Mandel, and E. Wolf (Plenum, New York, 1990).

<sup>6</sup>C. Weisbuch, M. Nishioka, A. Ishikawa, and Y. Arakawa, *Phys. Rev. Lett.* **69**, 3314 (1992).

<sup>7</sup>R. Houdre, C. Weisbuch, R. P. Stanley, U. Oesterle, P. Pellandini, and M. Illegems, *Phys. Rev. Lett.* **73**, 2043 (1994).

<sup>8</sup>T. A. Fisher, A. M. Afsar, D. M. Whittaker, M. S. Skolnick, J. S. Roberts, G. Hill, and M. A. Pate, *Phys. Rev. B* **51**, 2600 (1995).

<sup>9</sup>T. R. Nelson, J. P. Prineas, G. Khitrova, H. M. Gibbs, J. D. Berger, E. K. Lindmark, J.-H. Shin, H.-E. Shin, Y.-H. Lee, and P. Tayebati, *Appl. Phys. Lett.* **69**, 3031 (1996).

<sup>10</sup>T. B. Norris, J.-K. Rhee, C.-Y. Sung, Y. Arakawa, M. Nishioka, and C. Weisbuch, *Phys. Rev. B* **50**, 14663 (1994).

<sup>11</sup>J. Jacobson, S. Pau, H. Cao, G. Björk, and Y. Yamamoto, *Phys. Rev. A* **51**, 2542 (1995).

<sup>12</sup>H. Cao, J. Jacobson, G. Björk, S. Pau, and Y. Yamamoto, *Appl. Phys. Lett.* **66**, 1107 (1995).

<sup>13</sup>H. Cao, S. Jiang, S. Machida, T. Takiguchi, and Y. Yamamoto, *Appl. Phys. Lett.* **71**, 1461 (1997).

<sup>14</sup>R. Houdre, J. L. Gibernon, P. Pellandini, R. P. Stanley, U. Oesterle, W. Weisbuch, J. O'Gorman, B. Roycroft, and M. Illegems, *Phys. Rev. B* **52**, 7810 (1997).

<sup>15</sup>F. Jahnke, M. Kira, S. W. Koch, G. Khitrova, E. K. Lindmark, T. R. Nelson, D. V. Wick, J. D. Berger, O. Lyngnes, H. M. Gibbs, and K. Tai, *Phys. Rev. Lett.* **77**, 5257 (1996).

<sup>16</sup>H. Cao, S. Pau, J. M. Jacobson, G. Björk, Y. Yamamoto, and A. Imamoglu, *Phys. Rev. A* **55**, 4632 (1997).

<sup>17</sup>X. Fan, H. Wang, H. Q. Hou, and B. E. Hammons, *Phys. Rev. B* **56**, 3233 (1997).

<sup>18</sup>S. Jiang, S. Machida, Y. Takiguchi, H. Cao, and Y. Yamamoto, *Opt. Commun.* **145**, 91 (1998).

<sup>19</sup>S. Pau, G. Björk, J. M. Jacobson, H. Cao, and Y. Yamamoto, *Phys. Rev. B* **51**, 14437 (1995).